Supporting Information

Engineering high-valence nickel sites in Ni_3S_2/Ni_3Se_2 architectures enabling urea-assisted hydrogen evolution reaction

Taotao Ai[a, 1, *], Miaomiao Bai[b, 1], Weiwei Bao[a, *], Jie Han[a], Xueling Wei[a], Xiangyu Zou[a], Jungang Hou[b], Lizhai Zhang[a], Zhifeng Deng[a], Yuxin Zhang[c, *]

[a]National and Local Joint Engineering Laboratory for Slag Comprehensive Utilization and Environmental Technology, School of Materials Science and Engineering, Shaanxi University of Technology, Hanzhong 723000, Shaanxi, China.

[b]College of Chemistry and Materials Science, Northwestern University, Xi'an 710100, China.

[c]School of Chemical Engineering, Dalian University of Technology, Dalian 116024, China.

[d]College of Materials Science and Engineering, Chongqing University, Chongqing 400044, China.

[1]These authors contributed equally to this work

***Corresponding Author**

Taotao Ai, E-mail: aitaotao0116@126.com

Weiwei Bao, E-mail: baowei1834@163.com

Yuxin Zhang, E-mail: zhangyuxin@cqu.edu.cn

Number of pages: 27

Number of Figures: 16

Number of Tables: 1

List of Contents

Fig. S11. (a) EIS Nyquist plots of Ni_3S_2@Ni_3Se_2/NF, Ni_3S_2/NF, Ni_3Se_2/NF, Pt/C/NF and Bare NF. (b) Comparisons of the EIS parameter. (c) Polarization curves were recorded initially and after 2000 CV cycles for Ni_3S_2@Ni_3Se_2/NF.

Fig. S12. (a) Ni_3S_2@Ni_3Se_2/NF polarization curves in different electrolytes, (b) XRD, (c-d) SEM images and (e) EDX elemental mappings of Ni_3S_2@Ni_3Se_2/NF before and after stability test.

Fig. S13. The Faraday efficiency vs time plots in hydrogen production system assisted by urea electrocatalysis

Fig. S14. (a) Ni_3S_2 (211) surface structure model; and (b) the structure model of adsorption of H_2O; (c) Structure model of adsorption of H_2O (intermediate); (d) Structure model of adsorption of OH+H; (e) Structure model of adsorption H.

Fig. S15. (a) Ni_3Se_2 (211) surface structure model; and (b) the structure model of adsorption of H_2O; (c) Structure model of adsorption of H_2O (intermediate); (d) Structure model of adsorption of OH+H; (e) Structure model of adsorption H.

Fig. S16. (a) Ni_3Se_2 (211)/Ni_3S_2 (211) heterojunction surface structure model; and (b) the structure model of adsorption of H_2O; (c) Structure model of adsorption of H_2O (intermediate); (d) Structure model of adsorption of OH+H; (e) Structure model of adsorption H.

3. Supplementary Tables:

Supplementary Table S1. Comparison of the OER activity of Ni_3S_2@Ni_3Se_2/NF with other reported non-noble metal-based electrocatalysts in basic media (1 M KOH).

4. Notes and references

1. Experimental Section

1.1. Materials

Nickel nitrate hexahydrate ($Ni(NO_3)_2 \cdot 6H_2O$), vanadium trichloride (VCl_3), selenium dioxide (SeO_2), hydrazine hydrate ($N_2H_4 \cdot H_2O$), ethanol (C_2H_5OH), hydrochloric acid (HCl), ruthenic dioxide (RuO_2) and Nafion (5 wt%) were purchased from Sinopharm Chemical Reagent Co., Ltd. Milli-Q ultrapure water was used for all experiments. Nickel foam (NF) was used as the substrate. All chemicals were analytical grade and used as received without further purification.

1.2. Preparation of RuO_2 electrode on NF

A total of 1.2 mg RuO_2 powder was dispersed in 350 μL deionized water, 500 μL of ethanol, and 50 μL of 15 wt% Nafion solution through ultrasound for 30 min to form a uniform suspension. 300 μL of powder ink was loaded onto as-cleaned NF (1×1 cm^2), followed by the dry air at room temperature (Fig. S1e). The average mass loading of RuO_2 on NF is about 0.4 $mg \cdot cm^{-2}$.

1.3. General characterizations

The morphology of as-prepared catalysts was characterized by a field-emission scanning electron microscope (FESEM, JSM-7610F, 15 kV). The morphologies of samples were further confirmed by transmission electron microscope (TEM, Titan3 G2 60-300, 300 kV). The elemental distributions of the samples were characterized by the energy-dispersive X-ray spectroscopy (EDS) mapping affiliated with the TEM, and the EDS was also imaged from the TEM. Thermo Fisher Scientific K-Alpha was performed to get the X-ray photoelectron spectroscopy (XPS) data, using a monochromated source of X-rays (Mg Kα, photon energy 1253.6 eV) for excitation.

1.4. Electrochemical Test

All the electrochemical tests were proceeded in a standard three-electrode system by a CHI660E electrochemical station (CH Instruments, Inc., Shanghai) at room temperature. For detail, Ni_3S_2@Ni_3Se_2/NF was directly used as the working electrode, a graphite carbon rod was used as the counter electrode, and a mercury oxide electrode (Hg/HgO) was used as the reference electrode. All electrochemical measurements were carried out in a 1 M KOH solution. The measured potentials were transformed to a reversible hydrogen electrode (RHE) according to the equation: $E_{RHE} = E_{Hg/HgO} + 0.059 \times pH + 0.098$. The pH of 1 M KOH is measured to be 13.74. The OER measurements were recorded by linear sweep voltammetry (LSV) at a scan rate of 5 mV s^{-1}. Electrocatalytic stability was investigated by performing successive cyclic voltammetry (CV) sweeps in the voltage

range of 0-1.1 V at a scan rate of 40 mV/s. All polarization curves were corrected by *i-R* losses. The plots of electrochemical impedance spectroscopy (EIS) were measured with 5 mV amplitude in a frequency of 0.01 Hz ~ 100 kHz.

To obtain the effective electrochemical active surface area (ECSA) of electrocatalysts, a series of cyclic voltammetry (CV) measurements were executed first at various scan rates (5, 10, 15 mV s^{-1}, etc.). By plotting the difference of current density (J) between the anodic and cathodic sweeps ($J_{anodic}-J_{cathodic}$) against the scan rate, a linear trend was constructed. Then, the geometric double-layer capacitance (C_{dl}) was easily calculated.

2. **Supplementary Figures:**

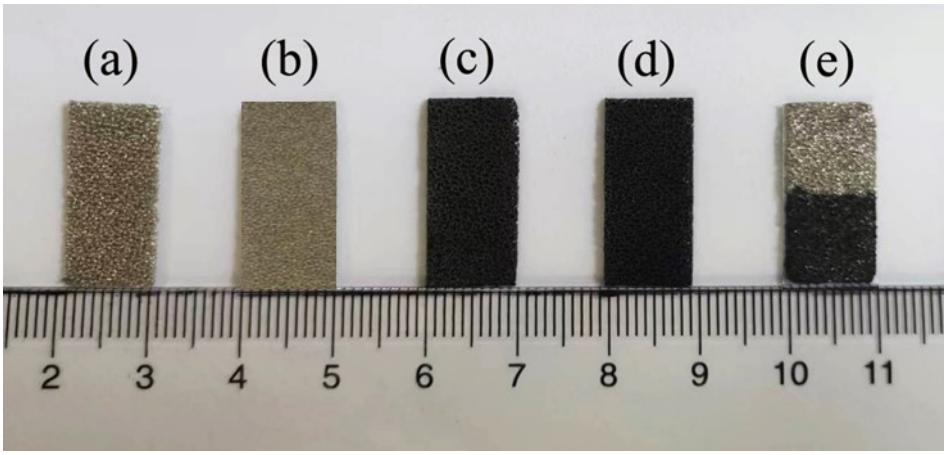

Fig. S1. Optical image of (a) the bare NF, (b) Ni_3S_2/NF, (c) Ni_3Se_2/NF, (d) Ni_3S_2@Ni_3Se_2/NF and (e) RuO_2/NF, respectively.

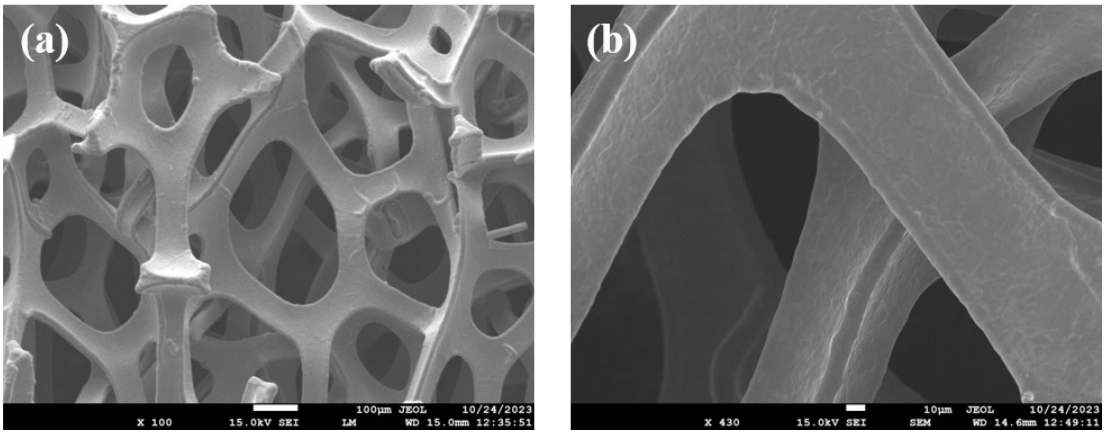

Fig. S2. The SEM images of bare NF (a) with low magnification, (b) with high magnification.

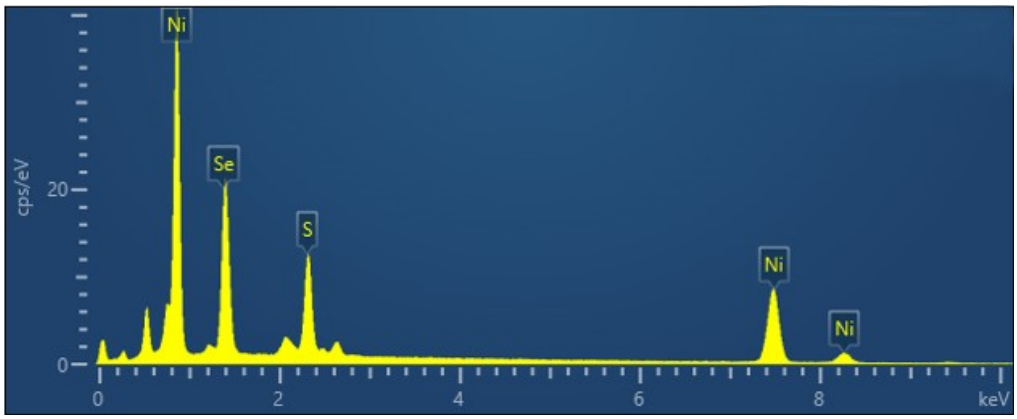

Fig. S3. The EDS spectrum of Ni_3S_2@Ni_3Se_2/NF electrode.

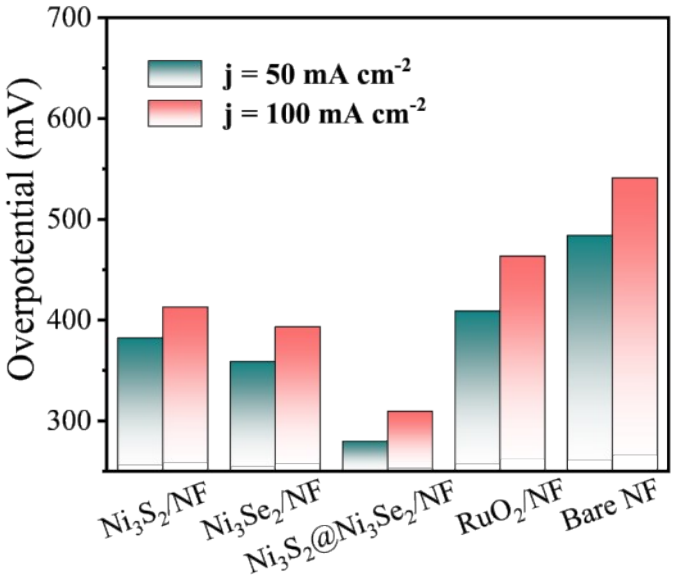

Fig. S4. Comparison of overpotentials of different current densities under OER test in 1 M KOH electrolyte.

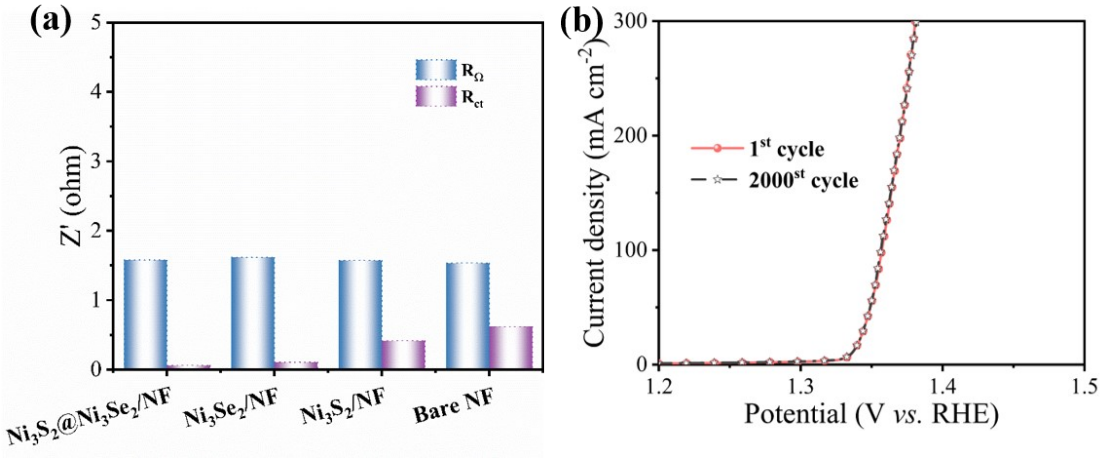

Fig. S5. (a) comparisons of the EIS parameter and (b) Polarization curves were recorded initially and after 2000 CV cycles for Ni_3S_2@Ni_3Se_2/NF of urea test in 1 M KOH + 0.33 M urea.

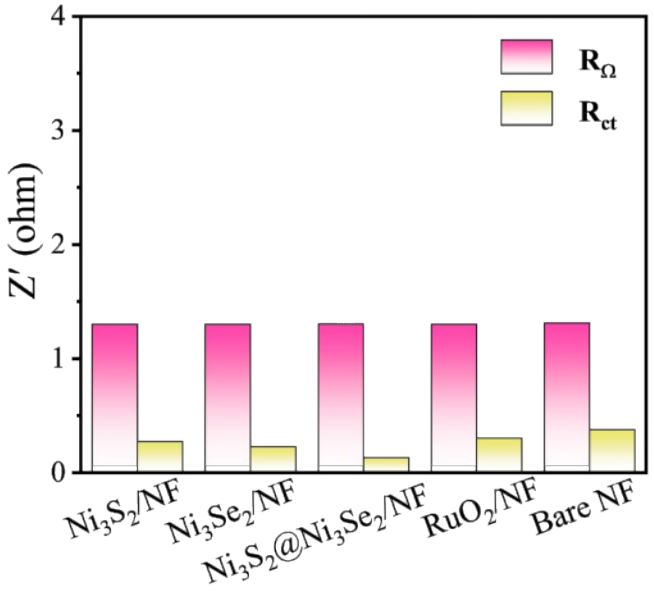

Fig. S6. Comparisons of the EIS parameter of OER test in 1.0 M KOH.

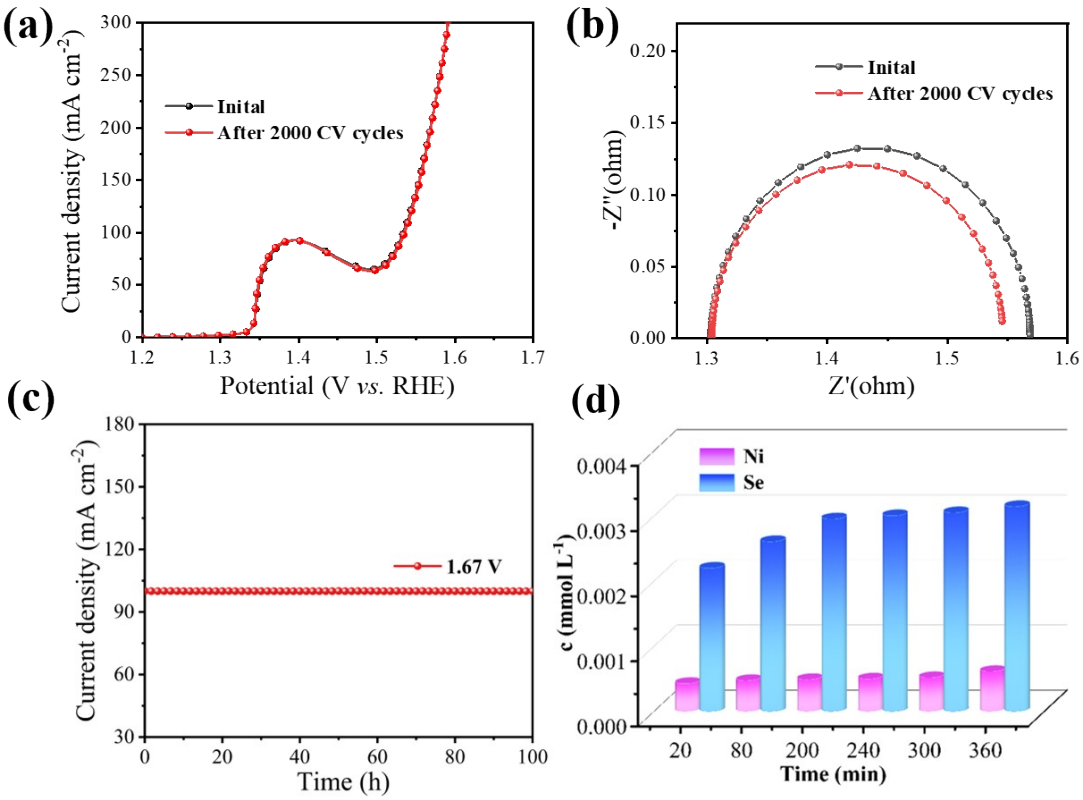

Fig. S7. Electrocatalytic stability. (a-b) Polarization curves and Nyquist plots of Ni_3S_2@Ni_3Se_2/NF electric catalyst initially as well as after 2000 CV cycles; (c) Chronopotentiometry curve of the Ni_3S_2@Ni_3Se_2/NF recorded at 1.67 V for 100 h; (d) Time-dependent concentration of dissolved Ni and Se in 1 M KOH.

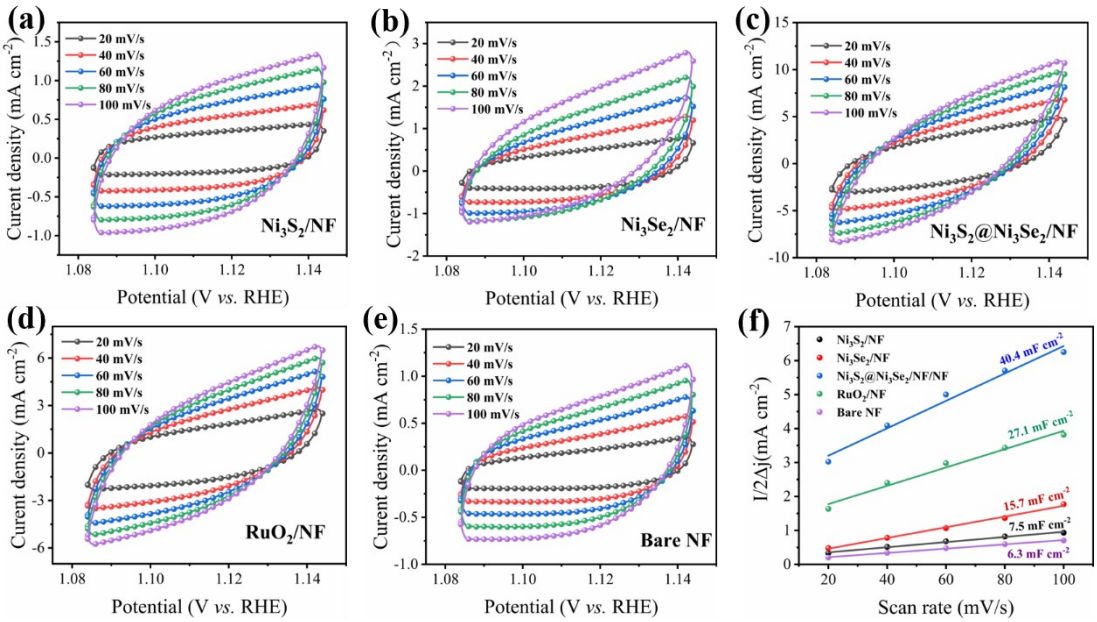

Fig. S8. Active site test CV curves of (a) Ni_3S_2/NF, (b) Ni_3Se_2/NF, (c) Ni_3S_2@Ni_3Se_2/NF, (d) RuO_2/NF and (e) Bare NF at different scanning rates in 1 M KOH; (e) current density as a function of scanning rate.

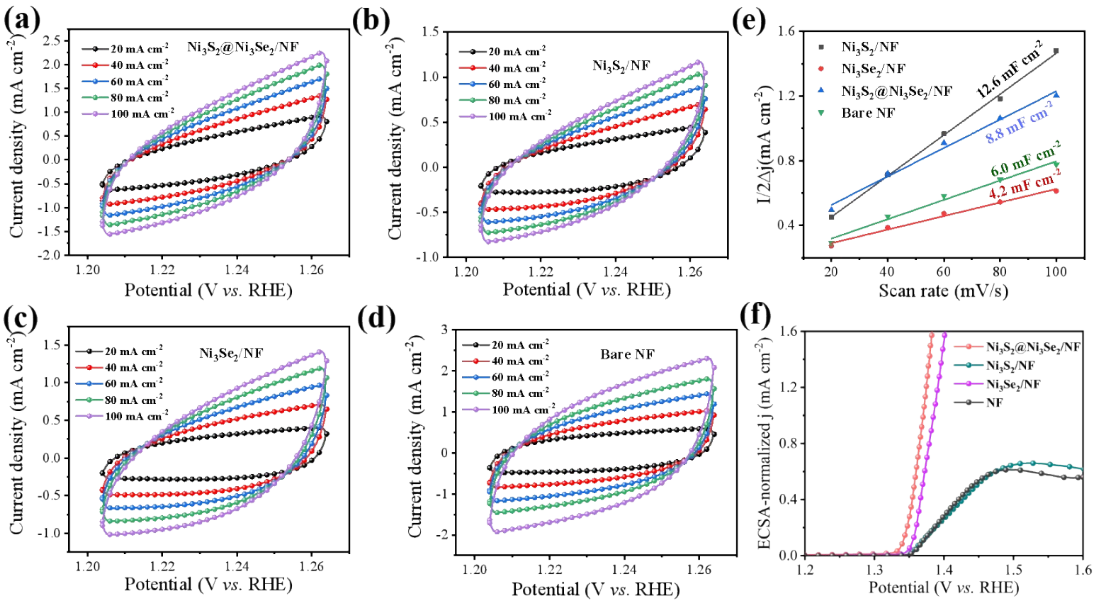

Fig. S9. Active site test CV curves of (a) Ni_3S_2@Ni_3Se_2/NF, (b) Ni_3S_2/NF (c) Ni_3Se_2/NF, (d) Bare NF at different scanning rates in 1 M KOH + 0.33 M urea; (e) current density as a function of scanning rate; (f) ECSA-normalized LSV curves.

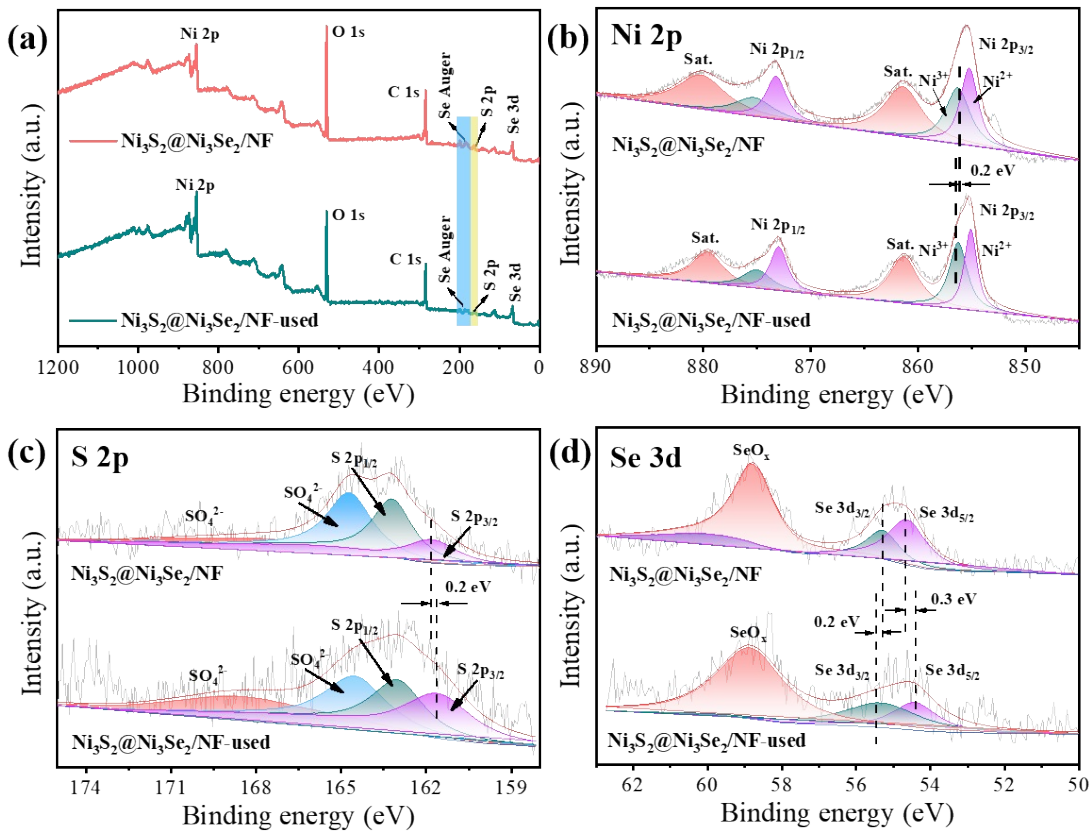

Fig. S10. (a) The physical characterization for Ni_3S_2@Ni_3Se_2/NF after OER test. The XPS survey spectrum of Ni_3S_2@Ni_3Se_2/NF, the spectra of (b) Ni 2p, (c) S 2p, and (d) Se 3d of Ni_3S_2@Ni_3Se_2/NF.

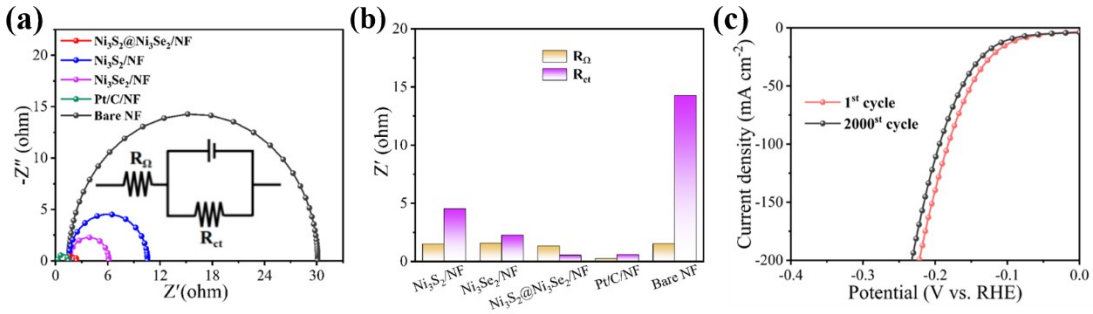

Fig. S11. (a) EIS Nyquist plots of Ni_3S_2@Ni_3Se_2/NF, Ni_3S_2/NF, Ni_3Se_2/NF, Pt/C/NF and Bare NF. (b) Comparisons of the EIS parameter. (c) Polarization curves were recorded initially and after 2000 CV cycles for Ni_3S_2@Ni_3Se_2/NF.

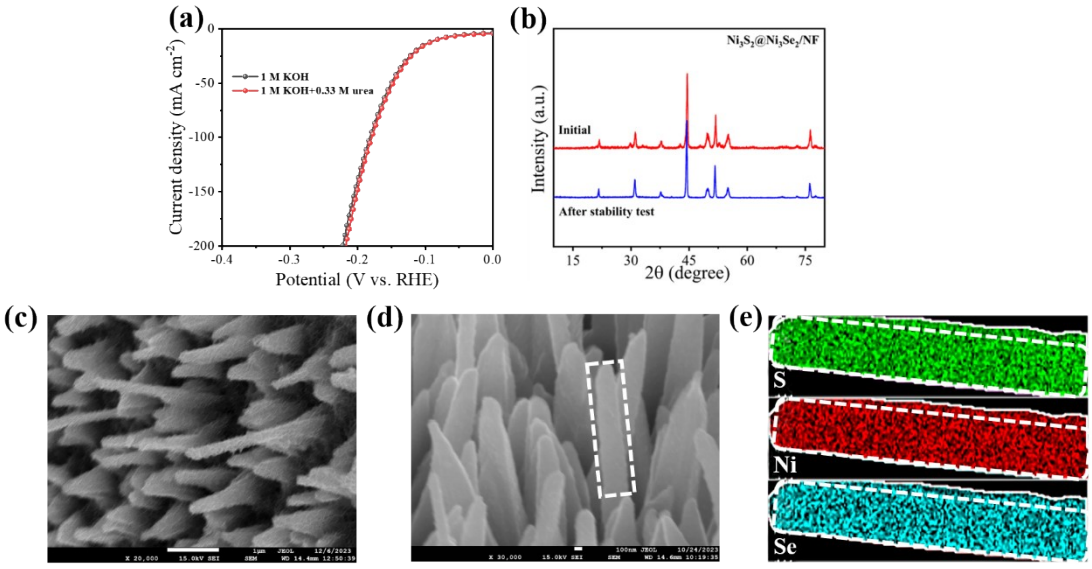

Fig. S12. (a) Ni_3S_2@Ni_3Se_2/NF polarization curves in different electrolytes, (b) XRD, (c-d) SEM images and (e) EDX elemental mappings of Ni_3S_2@Ni_3Se_2/NF before and after stability test.

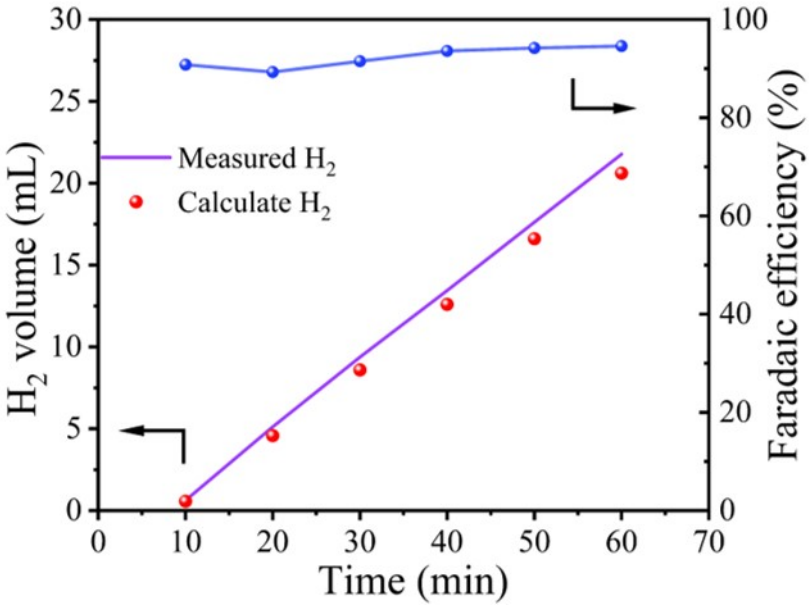

Fig. S13. The Faraday efficiency vs time plots in hydrogen production system assisted by urea electrocatalysis

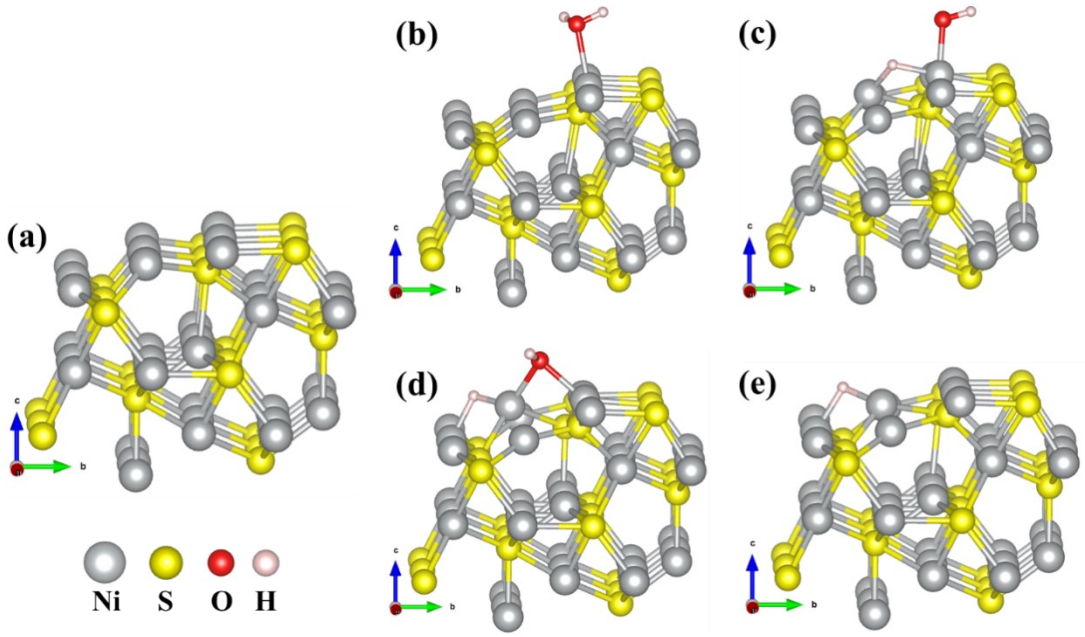

Fig. S14. (a) Ni_3S_2 (211) surface structure model; and (b) the structure model of adsorption of H_2O; (c) Structure model of adsorption of H_2O (intermediate); (d) Structure model of adsorption of OH+H; (e) Structure model of adsorption H.

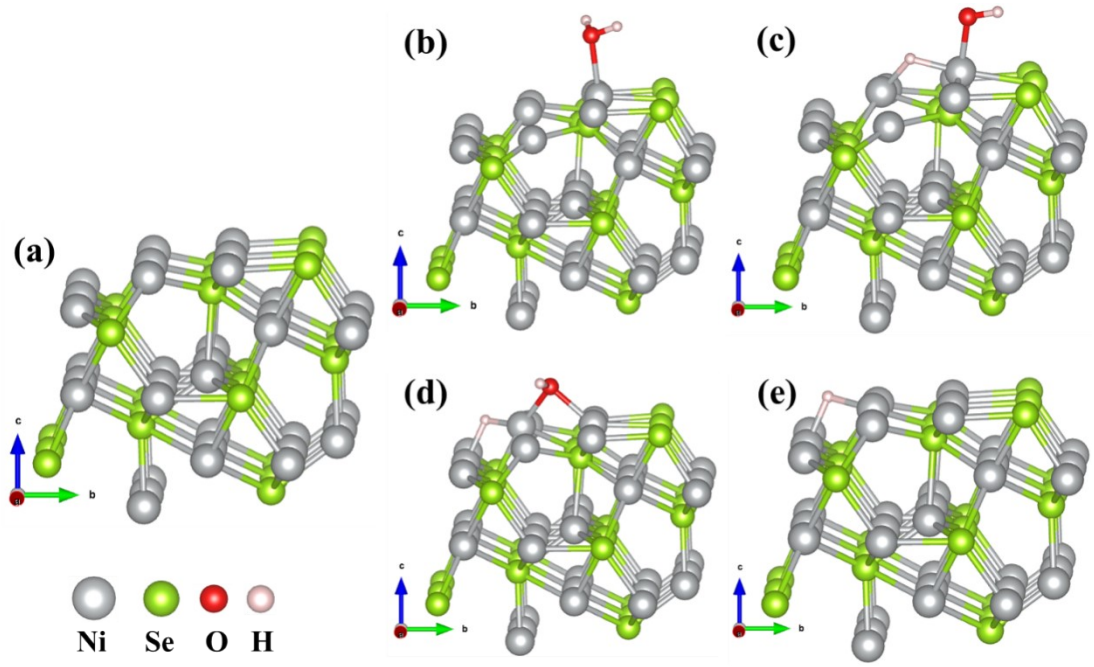

Fig. S15. (a) Ni_3Se_2 (211) surface structure model; and (b) the structure model of adsorption of H_2O; (c) Structure model of adsorption of H_2O (intermediate); (d) Structure model of adsorption of OH+H; (e) Structure model of adsorption H.

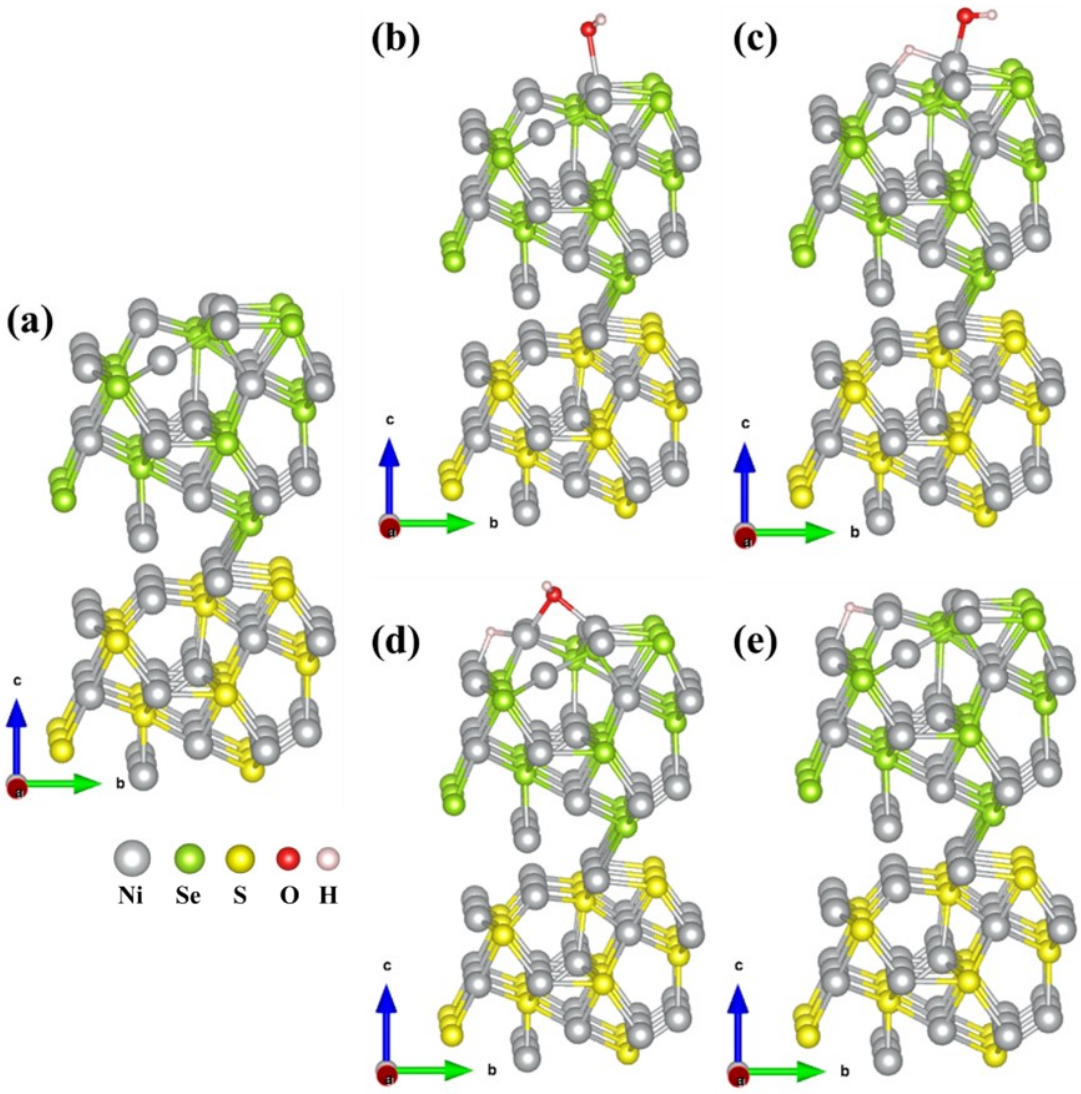

Fig. S16. (a) Ni_3Se_2 (211)/Ni_3S_2 (211) heterojunction surface structure model; and (b) the structure model of adsorption of H_2O; (c) Structure model of adsorption of H_2O (intermediate); (d) Structure model of adsorption of OH+H; (e) Structure model of adsorption H.

Supplementary Tables:

Supplementary Table S1 Comparison of the OER activity of Ni_3S_2@Ni_3Se_2/NF with other reported non-noble metal-based electrocatalysts in basic media (1 M KOH).

Catalysts	Current density (mA cm^{-2})	overpotential (mV)	Reference
Ni_3S_2@Ni_3Se_2/NF	10	234.89	This work
$CoSe_2$@Fe-CoO	10	280	[1] Journal of Materials Science & Technology, 2021, 78: 229-237.
$Ni_{0.85}$Se-O/CN	10	240	[2] Chemical Engineering Journal, 2023, 454: 140291.
$NiSe_2$@Fe-NiCo LDH	10	260	[3] International Journal of Hydrogen Energy, 2024, 51: 1154-1166.
$NiSe_2$@MoS_2	10	267	[4] RSC advances, 2021, 11(43): 26928-26936.
$Ni_{0.94}Fe_{0.06}Se_2$	10	279	[5] Journal of materials chemistry A, 2020, 8(16): 8113-8120.
P-$NiSe_2$@N-CNTs/NC	10	306	[6] Journal of Energy Chemistry, 2021, 60: 111-120.
$Fe_{0.2}Ni_{0.8}Se_2$	10	242	[7] Chemical Physics Letters, 2022, 808: 140126.
$Ni_{0.8}Fe_{0.2}Se_2$/CC	10	257	[8] Electrochimica Acta, 2022, 425: 140711.
$Fe_{0.5}Ni_{0.5}Se_2$	10	250	[9] Chemical Engineering Journal, 2023, 464: 142620.
Co-COF-C_4N	10	280	[10] Applied Catalysis B: Environmental, 2023, 325: 122366.
MoS_2	10	300	[11] Small, 2023, 19(14): 2207177.
MnSe@MWCNT	10	290	[12] Journal of Materials Chemistry A, 2022, 10(12): 6772-6784.

CuNi@NiSe	10	293	[13] Small, 2023, 19(33): 2301613.
S/N-CMF@FexCoyNi$_{1-x-y}$-MOF	10	296	[14] Advanced Materials, 2023, 35(19): 2207888.
Cu-(a-NiSe$_x$/c-NiSe$_2$)/TiO$_2$ NRs	10	339	[15] Chemical Engineering Journal, 2021, 422: 130048.
Fe_2O_3-Fe(Ni)S/C-200	10	264	[16] Small, 2023: 2307808.
$Cr_xNi_{1-x}Se_2$	10	272	[17] Nano Research, 2023: 1-10.
Ni SAs@S/N-CMF	10	221	[18] Advanced Materials, 2022, 34(35): 2203442.
$NiCl_2(CH_3CSNH_2)_4$	10	250	[19] Applied Catalysis B: Environmental, 2022, 312: 121389.
Mo-O_2S_2-C	10	324	[20] Journal of the American Chemical Society, 2022, 144(45): 20571-20581.

4. Notes and references

[1] M. Ramadoss, Y. F. Chen, Y. Hu, B. Wang, R. Jeyagopal, K. Marimuthu, X. Q. Wang, D. X. Yang, Hierarchically porous nanoarchitecture constructed by ultrathin $CoSe_2$ embedded Fe-CoO nanosheets as robust electrocatalyst for water oxidation, J. Mater. Sci. Technol. 78 (2021) 229-237.

[2] C. Zhang, W. Xu, S. T. Li, X. Z. Wang, Z. Y. Guan, M. L. Zhang, J. Wu, X. X. Ma, M. L. Wu, Y. F. Qi, Core-shell heterojunction engineering of $Ni_{0.85}Se$-O/CN electrocatalyst for efficient OER, Chem. Eng. J. 454 (2023) 140291.

[3] Q. R. Wang, C. Wang, X. Q. Du, X. S. Zhang, Combinational modulations of $NiSe_2$ nanodendrites by phase engineering and iron-doping towards efficient oxygen evolution reaction, Int. J. Hydrogen Energy, 51 (2024) 1154-1166.

[4] Y. Z. Huang, J. C. Huang, K. S. Xu, R. Geng, Constructing $NiSe_2$@MoS_2 nano-heterostructures on a carbon fiber paper for electrocatalytic oxygen evolution, RSC Adv. 11 (2021) 26928-26936.

[5] J. Zhou, L. W. Yuan, J. W. Wang, L. L. Song, Y. You, R. Zhou, J. J. Zhang, J. Xu, Combinational modulations of $NiSe_2$ nanodendrites by phase engineering and iron-doping towards an efficient oxygen evolution reaction, J. Mater. Chem. A. 8 (2020) 8113-8120.

[6] J. Yu, W. J. Li, G. B. Kao, C. Y. Xu, R. R. Chen, Q. Liu, J. Y. Liu, H. S. Zhang, J. Wang, In-situ growth of CNTs encapsulating P-doped $NiSe_2$ nanoparticles on carbon framework as efficient bifunctional electrocatalyst for overall water splitting, J. Energy Chem. 60 (2021) 111-120.

[7] C. Zhang, T. Li, Q. Z. Wei, Z. H. Cheng, J. Wu, X. X. Ma, Z. H. Chen, K. Y. Liu, T. Zhang, J. H. Liu, Fe-doped $NiSe_2$ nanoparticles as efficient and stable electrocatalysts for oxygen evolution reaction, Chem. Phys. Lett. 808 (2022) 140126.

[8] Z. M. Tian, Y. X. Liu, Q. C. Xu, Y. Y. Shi, C. X. Ma, B. Peng, G. Y. Liu, J. N. Yang, W. J. Zheng, Fe-doped $NiSe_2$ nanoarrays to boost electrocatalytic oxygen evolution reaction, Electrochim. Acta. 425 (2022) 140711.

[9] C. J. Xuan, Q. N. Xu, L. Han, B. S. Hou, Electronic structure exquisite modulation of $NiSe_2$ interface via rationally controlling Fe doping for boosting electrochemical oxygen evolution activity, Chem. Eng. J. 464 (2023) 142620.

[10] R. Zhang, W. S. Liu, F. M. Zhang, Z. D. Yang, G. L. Zhang, X. C. Zeng, COF-C_4N Nanosheets with uniformly anchored single metal sites for electrocatalytic OER: From theoretical screening to target synthesis, Appl. Catal. B Environ. 325 (2023) 122366.

[11] B. Chen, P. Hu, F. Yang, X. J. Hua, F. F. Yang, F. Zhu, R. Y. Sun, K. Hao, K. S. Wang, Z. Y. Yin, In situ porousized MoS_2 nano islands enhance HER/OER bifunctional electrocatalysis, Small. 19 (2023) 2207177.

[12] H. Singh, M. M. Hines, S. Chakravarty, M. Nath, Multi-walled carbon nanotube supported manganese selenide as a highly active bifunctional OER and ORR electrocatalyst, J. Mater. Chem. A. 10 (2022) 6772-6784.

[13] D. Cao, J. Shao, Y. H. Cui, L. P. Zhang, D. J. Cheng, Interfacial engineering of copper-nickel selenide nanodendrites for enhanced overall water splitting in alkali condition, Small. 19 (2023) 2301613.

[14] Y. F. Zhao, X. F. Lu, Z. P. Wu, Z. H. Pei, D. Y. Luan, X. W. D. Lou, Supporting Trimetallic Metal−Organic Frameworks on S/N‐Doped Carbon Macroporous Fibers for Highly Efficient Electrocatalytic Oxygen Evolution, Adv. Mater. 35 (2023) 2207888.

[15] K. R. Park, D. T. Tran, T. T. Nguyen, N. H. Kim, J. H. Lee, Copper-Incorporated heterostructures of amorphous NiSex/Crystalline $NiSe_2$ as an efficient electrocatalyst for overall water splitting, Chem. Eng. J. 422 (2021) 130048.

[16] W. Q. Zhang, J. Ying, H. W. Liu, Biomineralization of Sulfate−Reducing Bacteria In Situ−Induced Preparation of Nano Fe_2O_3‐Fe(Ni)S/C as High−Efficiency Oxygen Evolution Electrocatalyst, Small. 20 (2023) 2307808.

[17] H. F. Fan, D. X. Jiao, J. C. Fan, D. W. Wang, B. Zaman, W. Zhang, L. Zhang, W. Zheng, X. Q. Cui, Kinetically and thermodynamically expediting elementary steps via high-valence Cr-incorporated of nickel selenide for water electrolysis, Nano Res. 17 (2023) 1199-1208.

[18] Y. F. Zhao, Y. Guo, X. F. Lu, D. Y. Luan, X. J. Gu, X. W. D. Lou, Exposing Single Ni Atoms in Hollow S/N−Doped Carbon Macroporous Fibers for Highly Efficient Electrochemical Oxygen Evolution, Adv. Mater. 34 (2022) 2203442.

[19] X. Jia, H. J. Kang, X. X. Yang, Y. L. Li, K. Cui, X. H. Wu, W. Qin, G. Wu, Amorphous Ni (Ⅲ)-based sulfides as bifunctional water and urea oxidation anode electrocatalysts for hydrogen generation from urea-containing water, Appl. Catal. B Environ. 312 (2022) 121389.

[20] Y. Z. Zhao, Z. L. Zhang, L. Liu, Y. Wang, T. Wu, W. J. Qin, S. J. Liu, B. R. Jia, H. Y. Wu, D. Y. Zhang, X. H. Qu, G. G. Qi, E. P. Giannelis, M. L. Qin, S. J. Guo, S and O co-coordinated Mo single sites in hierarchically porous tubes from sulfur–enamine copolymerization for oxygen reduction and evolution, J. Am. Chem. Soc. 144 (2022) 20571-20581.